ACSES proceedings

Two-time Scale Analysis of a Ring of Coupled Vibratory Gyroscopes

Huy Vu, Antonio Palacios, Visarath In, Patrick Longhini,
and Joseph D. Neff

AP10-05

2010

Two-time Scale Analysis of a Ring of Coupled Vibratory Gyroscopes

Huy Vu[a], Prof. Antonio Palacios[a], Dr. Visarath In[b], Dr. Patrick Longhini[b], and Dr. Joseph D. Neff[b]
[a] *Nonlinear Dynamical Systems Group - Department of Mathematics, San Diego State University, San Diego, CA 92182*
[b] *Space and Naval Warfare Systems Center - Code 2363, 53560 Hull Street, San Diego, CA 92152-5001, USA.*

PACS numbers:

I. BI-DIRECTIONALLY COUPLED RING OF GYROSCOPES

A. Equations of Motion

We consider an array of N vibratory gyroscopes arranged in a ring configuration, coupled bidirectionally along the drive axis,

$$\begin{aligned} m_j\ddot{x}_j + c_{xj}\dot{x}_j + F_r(x_j) &= F_{ej}(t) \ + \ 2m_j\Omega_z\dot{y}_j + \sum_{k\to j} c_{jk}h(x_j,x_k) \\ m_j\ddot{y}_j + c_{yj}\dot{y}_j + F_r(y_j) &= \qquad\qquad - \ 2m_j\Omega_z\dot{x}_j, \end{aligned}$$

where h is the coupling function between gyroscopes j and k, the summation is taken over those gyroscopes k that are coupled to gyroscopes j, c_{jk} is a matrix of coupling strengths, and $A_d \to \varepsilon$. By assuming each gyroscope to be excited by the same external harmonic sine-wave signal with one driving frequency in the drive coordinate axis, i.e., $F_{ei} = F_d \sin w_d t$, and the coupling strength to be identical, i.e., $c_{jk} = \lambda$, the equations of motion take the form

$$\begin{aligned} m\ddot{x}_j + c\dot{x}_j + \kappa x_j + \mu x_j^3 &= \varepsilon \sin w_d t + 2m\Omega_z\dot{y}_j + \lambda(x_{j+1} - 2x_j + x_{j-1}) \\ m\ddot{y}_j + c\dot{y}_j + \kappa y_j + \mu y_j^3 &= -2m\Omega_z\dot{x}_j. \end{aligned} \tag{1}$$

B. Computational Bifurcation Analysis

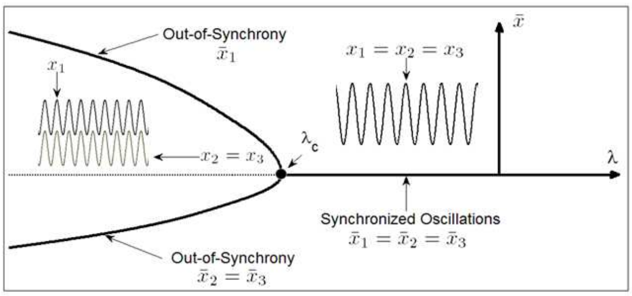

FIG. 1: One-parameter bifurcation diagram illustrating the existence and stability properties of synchronized periodic oscillations in a ring of three vibratory gyroscopes bi-directionally coupled (n=3).

In figure (1), the onset of oscillations governed by the model equations (1) occurs when the coupling strength exceeds a critical value, which we denote by λ_c. When $\lambda < \lambda_c$, there are two stable periodic solutions and one unstable periodic solution. As λ increases towards λ_c, the two non-zero mean periodic solution and the zero-mean periodic solution merge in a supercritical pitchfork bifurcation. Past λ_c, only the zero-mean periodic solution exists and becomes globally asymptotically stable. The oscillations along the sensing axis are, however, unaffected by the change in coupling. They are always stable and completely synchronized with one another though they are out-of-phase by π with those of the driving axis due to the sign difference in the Coriolis force terms.

C. Two-Time Scale Analysis

In order to determine an expansion for $x_j(t)$ and $y_j(t)$ uniformly valid for large times, we introduce two times scales: a fast-time scale $\xi = w_d t$ and a slow-time scale $\eta = \varepsilon t$. In order to introduce these two-time scales into (1), we need expression for the first and second derivatives of x and y with respect to t, which we obtain by using the chain rule:

$$\frac{dx_j}{dt} = w_d \frac{\partial x_j}{\partial \xi} + \varepsilon \frac{\partial x_j}{\partial \eta}, \quad \frac{d^2 x_j}{dt^2} = w_d^2 \frac{\partial^2 x_j}{\partial \xi^2} + 2\varepsilon w_d \frac{\partial^2 x_j}{\partial \xi \partial \eta} + \varepsilon^2 \frac{\partial^2 x_j}{\partial \eta^2}, \tag{2a}$$

$$\frac{dy_j}{dt} = w_d \frac{\partial y_j}{\partial \xi} + \varepsilon \frac{\partial y_j}{\partial \eta}, \quad \frac{d^2 y_j}{dt^2} = w_d^2 \frac{\partial^2 y_j}{\partial \xi^2} + 2\varepsilon w_d \frac{\partial^2 y_j}{\partial \xi \partial \eta} + \varepsilon^2 \frac{\partial^2 y_j}{\partial \eta^2}. \tag{2b}$$

We also expand x_j and y_j in a truncated Fourier series of ε:

$$x_j = x_{0j} + \varepsilon(x_{1j} + A_{1j}\cos\xi + B_{1j}\sin\xi) + \varepsilon^2(x_{2j} + A_{2j}\cos\xi + B_{2j}\sin\xi + E_{2j}\cos 2\xi + F_{2j}\sin 2\xi) + \dots \tag{3a}$$

$$y_j = y_{0j} + \varepsilon(y_{1j} + C_{1j}\cos\xi + D_{1j}\sin\xi) + \varepsilon^2(x_{2j} + C_{2j}\cos\xi + D_{2j}\sin\xi + G_{2j}\cos 2\xi + H_{2j}\sin 2\xi) + \dots \tag{3b}$$

Substituting (2) and (3) into (1) and neglecting terms of $O(\varepsilon^3)$, we get, after collecting equal powers of ε, a set of partial differential equations for each order terms. The expressions for $O(1)$ are,

$$m w_d^2 \frac{\partial^2 x_{0j}}{\partial \xi^2} + c w_d \frac{\partial x_{0j}}{\partial \xi} + \kappa x_{0j} + \mu x_{0j}^3 = 2m\Omega_z w_d \frac{\partial y_{0j}}{\partial \xi} + \lambda(x_{0,j+1} - 2x_{0j} + x_{0,j-1}), \tag{4a}$$

$$m w_d^2 \frac{\partial^2 y_{0j}}{\partial \xi^2} + c w_d \frac{\partial y_{0j}}{\partial \xi} + \kappa y_{0j} + \mu y_{0j}^3 = -2m\Omega_z w_d \frac{\partial x_{0j}}{\partial \xi}. \tag{4b}$$

By collecting $O(\varepsilon)$ terms, we get:

$$m w_d^2 \frac{\partial^2 x_{1j}}{\partial \xi^2} + c w_d \frac{\partial x_{1j}}{\partial \xi} + \kappa x_{1j} + 3\mu x_{0j}^2 x_{1j} = 2m\Omega_z w_d \frac{\partial y_{1j}}{\partial \xi} \quad + \lambda(x_{1,j+1} - 2x_{1j} + x_{1,j-1}), \tag{5a}$$

$$m w_d^2 \frac{\partial^2 y_{1j}}{\partial \xi^2} + c w_d \frac{\partial y_{1j}}{\partial \xi} + \kappa y_{1j} + 3\mu y_{0j}^2 y_{1j} = -2m\Omega_z w_d \frac{\partial x_{1j}}{\partial \xi}, \tag{5b}$$

$$m w_d^2 \frac{\partial^2 X_{1j}}{\partial \xi^2} + c w_d \frac{\partial X_{1j}}{\partial \xi} + \kappa X_{1j} + 3\mu x_{0j}^2 X_{1j} = \sin w_d t + 2m\Omega_z w_d \frac{\partial Y_{1j}}{\partial \xi} \quad + \lambda(X_{1,j+1} - 2X_{1j} + X_{1,j-1}), \tag{5c}$$

$$m w_d^2 \frac{\partial^2 Y_{1j}}{\partial \xi^2} + c w_d \frac{\partial Y_{1j}}{\partial \xi} + \kappa Y_{1j} + 3\mu y_{0j}^2 Y_{1j} = -2m\Omega_z w_d \frac{\partial X_{1j}}{\partial \xi}, \tag{5d}$$

where $X_{1j} = A_{1j}\cos\xi + B_{1j}\sin\xi$ and $Y_{1j} = C_{1j}\cos\xi + D_{1j}\sin\xi$.

Collecting $O(\varepsilon^2)$ terms we get:

$$m w_d^2 \frac{\partial^2 x_{2j}}{\partial \xi^2} + c w_d \frac{\partial x_{2j}}{\partial \xi} + \kappa x_{2j} + 3\mu x_{0j}(x_{0j} x_{2j} + \frac{3}{2}||X_{1j}||^2) = 2m\Omega_z w_d \frac{\partial y_{2j}}{\partial \xi} + \lambda(x_{2,j+1} - 2x_{2j} + x_{2,j-1}), \tag{6a}$$

$$m w_d^2 \frac{\partial^2 y_{2j}}{\partial \xi^2} + c w_d \frac{\partial y_{2j}}{\partial \xi} + \kappa y_{2j} + 3\mu y_{0j}^2 y_{2j} = -2m\Omega_z w_d \frac{\partial x_{2j}}{\partial \xi}, \tag{6b}$$

$$m w_d^2 \frac{\partial^2 X_{2j}}{\partial \xi^2} + c w_d \frac{\partial X_{2j}}{\partial \xi} + \kappa X_{2j} + 3\mu x_{0j}(x_{0j} X_{2j} + \frac{3}{2}||X_{1j}||^2) = 2m\Omega_z w_d \frac{\partial Y_{2j}}{\partial \xi} + \lambda(X_{2,j+1} - 2X_{2j} + X_{2,j-1}), \tag{6c}$$

$$m w_d^2 \frac{\partial^2 Y_{2j}}{\partial \xi^2} + c w_d \frac{\partial Y_{2j}}{\partial \xi} + \kappa Y_{2j} + 3\mu y_{0j}^2 Y_{2j} = -2m\Omega_z w_d \frac{\partial X_{2j}}{\partial \xi}, \tag{6d}$$

where $||X_{1j}||^2 = A_{1j}^2 + B_{1j}^2$, $X_{2j} = A_{2j}\cos\xi + B_{2j}\sin\xi + E_{2j}\cos 2\xi + F_{2j}\sin 2\xi$ and $Y_{2j} = C_{2j}\cos\xi + D_{2j}\sin\xi + G_{2j}\cos 2\xi + H_{2j}\sin 2\xi$.

We solve the resulting system of equations analytically via Maple which yields a unique solution. Finally, we can now use (3) to reconstruct, up to $O(\varepsilon^2)$, the vibrations along the driving, $x_j(t)$, and sensing, $y_j(t)$, modes. Figures 2 and 3 compare the time-series of these reconstructed asymptotic solutions for a ring of three gyroscopes against those from numerical simulations. When $\lambda > \lambda_c$, the oscillations of the driving modes become entrained with one another,

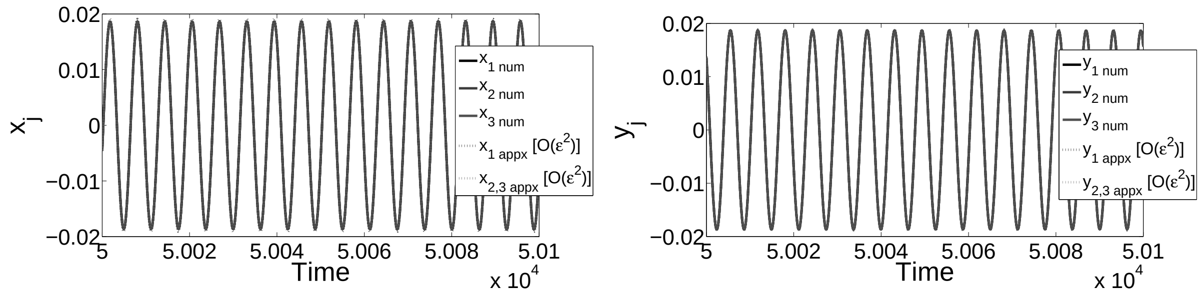

FIG. 2: Comparison of asymptotic approximation up to $O(\varepsilon^2)$ term and numerical solutions. Passed the critical coupling strength λ_c. Parameters are: $A_d = 0.001$, $\lambda = -0.883$, $\Omega_z = 308$.

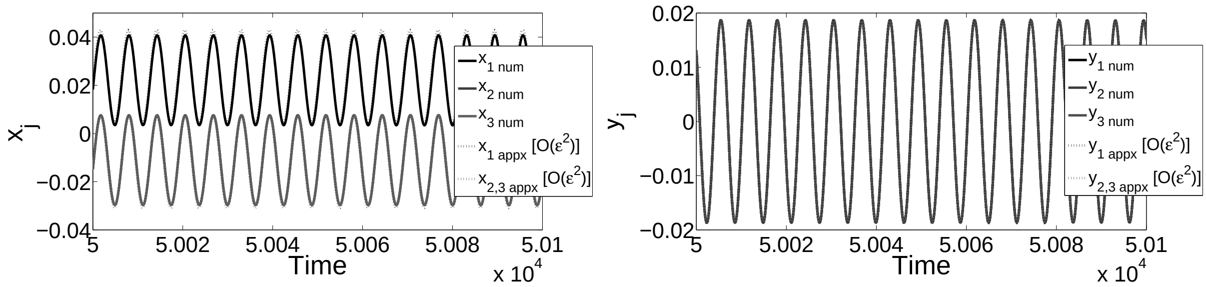

FIG. 3: Solutions are obtained analytically through the asymptotic approximation up to $O(\varepsilon^2)$ compared against numerical simulations, as λ is slightly to the left of the critical coupling strength λ_c. Parameters are: $A_d = 0.001$, $\lambda = -0.884$, $\Omega_z = 308$.

giving rise to a globally asymptotic stable synchronized state. When $\lambda < \lambda_c$, however, both numerical solutions and asymptotic solutions of the driving modes oscillate with non-zero mean.

D. Onset of Synchronization

We estimate the onset of synchronization of the coupled gyroscope system by averaging the values at which the solutions for $x_j(t)$, given by the asymptotic expressions (3), touch zero. Direct calculations yield the critical values in parameters space $(A_{dc}, \lambda_c, \Omega_{zc})$, in which we write A_{dc} as a function of λ_c and Ω_{zc}, through

$$\begin{aligned}
A_{dc} &= \frac{1}{3}(A_{d_{c1}} + A_{d_{c2}} + A_{d_{c3}}),\\
A_{d_{c1}} &= \frac{-||X_{11}|| - \sqrt{||X_{11}||^2 - 4(x_{21} - ||X_{21}||)x_{01}}}{2(x_{21} - ||X_{21}||)}\\
A_{d_{c2}} &= \frac{-||X_{12}|| - \sqrt{||X_{12}||^2 - 4(x_{22} - ||X_{22}||)x_{01}}}{2(x_{21} - ||X_{22}||)}\\
A_{d_{c3}} &= A_{d_{c2}}.
\end{aligned}$$

where $||X_{11}|| = \sqrt{A_{11}^2 + B_{11}^2}$, $||X_{12}|| = \sqrt{A_{12}^2 + B_{12}^2}$, $||X_{21}|| = \sqrt{E_{21}^2 + F_{21}^2}$, $||X_{22}|| = \sqrt{E_{22}^2 + F_{22}^2}$. Figure 4 shows a direct comparison of the analytical expression for A_{dc} as a function of coupling strength λ_c, with Ω_z held fixed, against the onset of synchronization obtained through numerical simulations with the aid of the continuation package AUTO. A similar curve is obtained for larger values of Ω_z but with a slight vertical shift that increases as Ω_z increases. In other words, the larger the Coriolis force is the larger the amplitude of the driving force that is required to sustain the synchronization state of the coupled gyroscope system.

Holding now A_d fixed, while varying Ω_z, we obtain the locus of the pitchfork bifurcation λ_c as a function of Ω_z. The locus traces a two-parameter bifurcation diagram shown in Fig. 5.

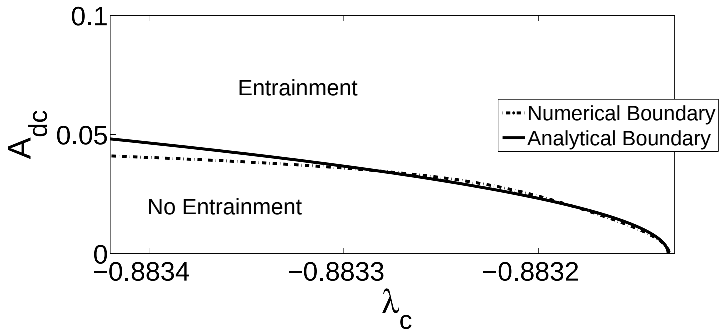

FIG. 4: Two-parameter bifurcation diagram outlines the region of parameter space (A_d, λ) where the vibrations of a system of three gyroscopes, coupled bi-directionally, become completely synchronized.

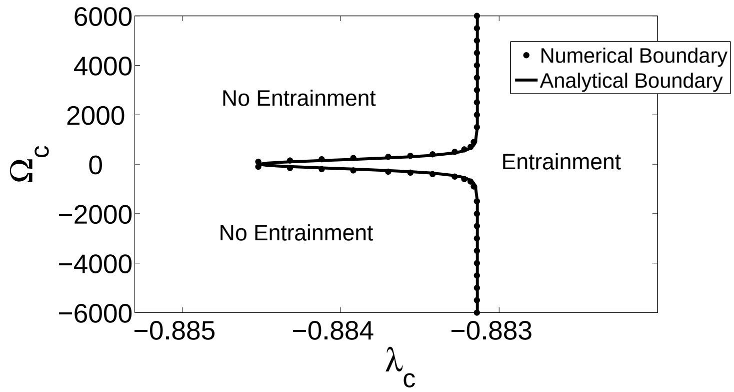

FIG. 5: Two-parameter bifurcation diagram shows the region of parameter space (Ω_z, λ) where the vibrations of a system of three gyroscopes, coupled bi-directionally, become completely synchronized but A_d is held fixed at 0.001.

II. EFFECTS OF NOISE

A. Assumption, Condition and Numerical Algorithm

With the expectation of noise occurred in the Coupled Inertial Navigation System to arise from the two main sources: fluctuations in the mass of individual coupled gyroscopes caused by material impurity and contamination of a target signal. Informal discussions with experimentalists suggest that a range $m_i = 1.0E-09 \pm 10\%$ is actually reasonable. We assume Gaussian band-limited noise having zero mean, correlation time τ_c (usually $\tau_F << \tau_c$, where τ_F is the time constant of each individual gyroscope, so that noise does not drive its response), and variance σ^2. From a modeling point of view, colored noise $\eta(t)$ that contaminates the signal should appear as an additive term in the sensing axis, leading to a stochastic (Langevin) version of the model equations,

$$\begin{aligned} m_j\ddot{x}_j + c\dot{x}_j + \kappa x_j + \mu x_j^3 &= A_d \sin w_d t + 2m_j\Omega_z\dot{y}_j + \lambda(x_{j+1} - x_j), \\ m_j\ddot{y}_j + c\dot{y}_j + \kappa y_j + \mu y_j^3 &= -2m_j\Omega_z\dot{x}_j, \\ \frac{d\eta}{dt} &= -\frac{\eta_j}{\tau_c} + \frac{\sqrt{2}}{\tau_c}\xi(t). \end{aligned} \tag{7}$$

B. Robustness

In this work we will consider the situation wherein the different noise terms, $\eta_i(t)$, are uncorrelated; however, for simplicity, we will assume them to have the same intensity D. Each (colored) noise $\eta_i(t)$ is characterized by

$< \eta_i(t) >= 0$ and $< \eta_i(t)\eta_i(s) >= (D/\tau_c) \times exp[-|t-s|/\tau_c] >$, where $D = \sigma^2\tau_c^2/2$ is the noise intensity, $\xi(t)$ is a gaussian white noise function of zero mean, and the "white" limit is obtained for vanishing τ_c; in practice, however, the noise is always band-limited. The new computational bifurcation diagrams (not shown for brevity) are very similar to the one- and two-parameter diagrams shown in Fig. (1), Fig. (4), and Fig. (5), except that now the critical values of coupling strength λ_c as well as Ω_c and A_{dc} are slighted shifted with respect to those of the identical system. Each ensemble consisted of M = 100 simulation samples with random fluctuations in mass and noise intensities. The phase of each individual j gyroscope was calculated through $\alpha_j = \arctan(-\dot{y}_j/w_d y_j)$. Then the phase drift on that individual gyroscope was obtained as the difference between its phase with noise and its phase without noise, i.e., $\theta_j = \alpha_j^{noise} - \alpha_j^{no\ noise}$. Finally, the average phase drift $\theta_j(t) = (1/MN)\sum_{j=1}^{MN}\theta_j$ of the entire ensemble was calculated for both cases, uncoupled and coupled ensembles. Figure 13 shows, in particular, the phase drift of an ensemble of three individual gyroscopes and the phase drift of a similar ensemble but with coupling.

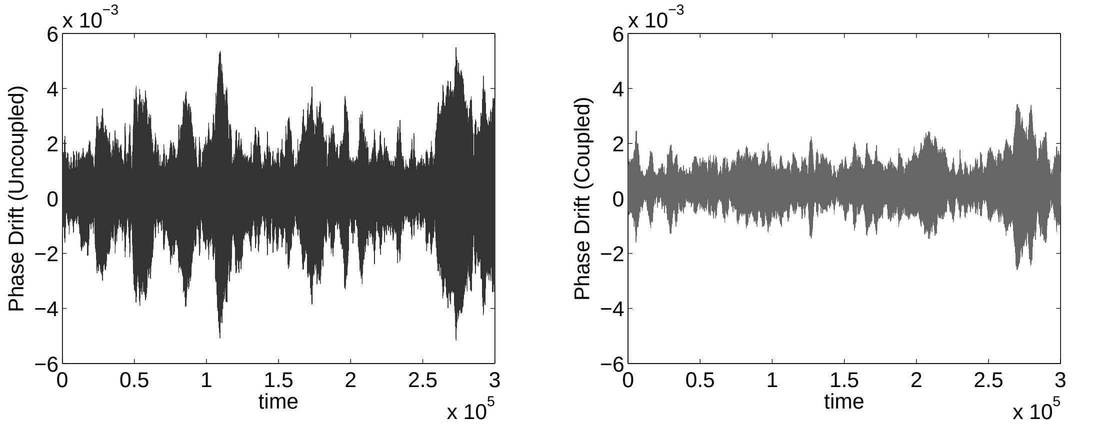

FIG. 6: Comparison of phase drift between (left) three uncoupled gyroscopes and (right) three coupled gyroscope system. Parameters are: $A_d = 0.001$, $\Omega_z = 100$, and mass $m_j = 1.0E-09 \pm 10\%$ with noise intensities, $D = \pm 1.0E-09$.

To calculate the actual reduction factor we first compute the interquartile range (IQR) of both uncoupled and coupled ensembles. The IQR measures the phase drift variation from the 25% percentile to the 75% percentile. The reduction factor is then the ratio IQR(θ^c) / IQR(θ^u), where the superscript indicates whether the gyroscopes are coupled or uncoupled, respectively. Figure (7) shows the resulting reduction factors for various network sizes. Careful examination of the average amplitude response of an ensemble of coupled gyroscopes [Fig. (7)] reveals that the amplitude of the sensing axis is dynamically dependent on the number N of gyroscopes and the coupling strength λ. In fact, the largest amplitudes are achieved in the vicinity of N = 8.

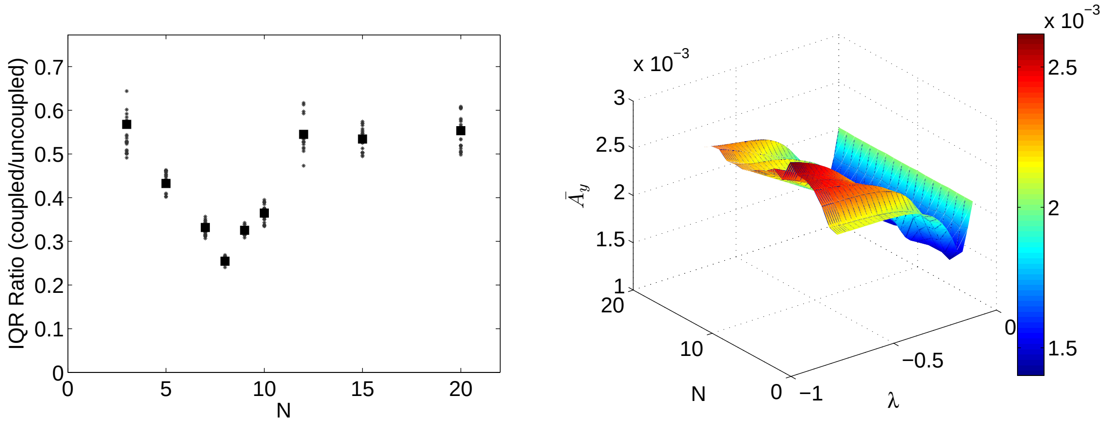

FIG. 7: (a)[Left] Reduction factor in the phase drift of a coupled gyroscope system with the interquartile range of ensembles between 80 and 100 samples. Parameters are: $A_d = 0.001$, $\Omega_z = 100$, and mass $m_j = 1.0E-09 \pm 10\%$ with noise intensities, $D = \pm 1.0E-09$. (b) [Right] Average amplitude response of sensing axis of ensembles of coupled gyroscopes with various sizes and coupling strengths. Parameters are: $A_d = 0.001$, $\Omega_z = 100$, and mass $m_j = 1.0E-09 \pm 10\%$ without noise.